ARTICLE

Quantum teleportation-based state transfer of photon polarization into a carbon spin in diamond

Kazuya Tsurumoto[1], Ryota Kuroiwa[1], Hiroki Kano[1], Yuhei Sekiguchi [1] & Hideo Kosaka [1]

Quantum teleportation is a key principle for quantum information technology. It permits the transfer of quantum information into an otherwise inaccessible space, while also permitting the transfer of photon information into a quantum memory without revealing or destroying the stored quantum information. Here, we show reliable quantum state transfer of photon polarization into a carbon isotope nuclear spin coupled to a nitrogen-vacancy center in diamond based on photon-electron Bell state measurement by photon absorption. The carbon spin is first entangled with the electron spin, which is then permitted to absorb a photon into a spin-orbit correlated eigenstate. Detection of the electron after relaxation into the spin ground state allows post-selected transfer of arbitrary photon polarization into the carbon memory. The quantum state transfer scheme allows individual addressing of integrated quantum memories to realize scalable quantum repeaters for long-haul quantum communications, and distributed quantum computers for large-scale quantum computation and metrology.

[1] Yokohama National University, 79-5 Tokiwadai, Hodogaya, Yokohama 240-8501, Japan. Correspondence and requests for materials should be addressed to H.K. (email: kosaka-hideo-yp@ynu.ac.jp)

Quantum teleportation[1,2] is a widely used principle for quantum information technologies including quantum communication[3–5] and quantum computing[6]. Long-haul quantum communication requires quantum repeaters[7–13] based on quantum teleportation to transfer a quantum bit or qubit into a distant site without revealing the qubit state. Quantum computation[6] also requires quantum teleportation not only for one-way quantum computing but also for quantum blind computing[14] to securely transfer input and output data via quantum communication. Finally, quantum teleportation is also in demand for the quantum storage of highly confidential data, such as DNA data, that are securely transferred by photons into quantum memories.

We have recently demonstrated the transfer of photon polarization into a nitrogen nuclear spin in a single nitrogen-vacancy (NV) center in diamond[11]. Delteil et al. have also demonstrated heralded absorption of a single photon color qubit in a single quantum dot[12]. However, the stored information is limited to only one nuclear spin per one NV center or one electron spin per one quantum dot, which is a big obstacle for scaling up the memory size. On the other hand, there exist a large number of carbon isotopes (^{13}C), which also have nuclear spins, within the reach of a nitrogen-vacancy center via a hyperfine interaction even in diamond with a natural abundance of ^{13}C (1.1%), and the number can be increased by isotope enrichment technology[15]. The stored qubits in carbon nuclear spins must be independent of each other and individually addressable[16–21]. We have also recently demonstrated that the quantum state of isolated carbon nuclear spins weakly coupled to the NV center's electron can be ideally maintained by the geometric spin echo based on time reversal under a zero magnetic field[22]. However, it is hard to initialize and manipulate a spin-half carbon nuclear spin under a zero magnetic field, in contrast to the spin-1 nitrogen, which has a zero-field split state to allow manipulation by a resonant microwave.

In the present work, we successfully initialize and manipulate a carbon nuclear spin using nitrogen as a nanomagnet to lift the degeneracy of the electron while maintaining a magnetic field of zero at the carbon nuclear spin, then transfer the polarization state of photons into the spin quantum state of the thus-prepared carbon nuclear spin. We experimentally demonstrate that the state transfer process shows quantum nature and thus the transfer fidelity exceeds the classical limit, based on the quantum process tomography technique.

Results

Principle. Quantum teleportation consists in the preparation of an entanglement and the measurement in the Bell basis, resulting in post-selective transfer of the quantum state (Fig. 1a). In the current demonstration, we first prepare an entanglement between electron spin and carbon nuclear spin, and then measure photon polarization and electron spin in the Bell basis by photon absorption[23] to transfer the photon polarization state into the carbon spin state (Fig. 1b, c). In the practical protocol of the one-way quantum repeater system with an NV center at each node, the photon is emitted from one node, leaving an electron entangled with the emitted photon[24] (Fig. 1d). The success of the photon storage in the other node establishes the entanglement between two adjacent nodes.

A negatively charged NV center in diamond consists of a nitrogen impurity (^{14}N) and an adjacent vacancy (V), where the triplet state electron (e) is localized (Fig. 1b). Both the electron and the nitrogen nucleus show a spin 1 property constituting a V-type three-level system with two degenerate $m_{s,I} = \pm 1$ states (denoted $| \pm 1\rangle_{e,N}$), which constitute a logical qubit called a geometric spin qubit[22,23,25–29], and an $m_{s,I} = 0$ state

(denoted $|0\rangle_{e,N}$), which constitute an ancilla. These are split by a zero-field splitting of around 2.87 GHz for the electron and a nuclear quadrupole splitting of around 4.95 MHz for the nitrogen. On the other hand, a carbon nuclear spin (^{13}C), weakly coupled to the electron via a hyperfine interaction (0.9 MHz in this demonstration), shows a spin half property constituting a two-level system with two degenerate $m_I = \pm 1/2$ states (denoted $|\uparrow\rangle_C, |\downarrow\rangle_C$) under a zero magnetic field (Fig. 1c). We utilize the nitrogen as a nanomagnet localized at the vacancy.

To prepare the spin entanglement between the electron and carbon nuclear spin, we first initialize them into $|0\rangle_e|\uparrow\rangle_C$. Although it is hard to initialize the carbon nuclear spin under a zero magnetic field, the nuclear quadrupole splitting of the nitrogen nuclear spin with the help of the polarized electron spin enables the polarization into $|+1\rangle_N$, which is used as a nanomagnet to apply a local magnetic field on the electron to initialize the carbon nuclear spin (Fig. 1c) with the following sequence (see Supplementary Note 1). The coherent population trapping (CPT) using a red light resonantly exciting the electron into a spin-orbit correlated eigenstate $|A_2\rangle = \frac{1}{\sqrt{2}}(|+1, -1\rangle_{l,e} + |-1, +1\rangle_{l,e})^{23,24}$ (l and e, respectively denote orbital and spin angular momentums of an electron) with the right circular polarization $|+1\rangle_p$ first polarizes the electron into $|+1\rangle_e^{23}$, which is then transferred into the nitrogen nuclear spin to polarize into $|+1\rangle_N$ (purple line in Fig. 2a). The degeneracy of the electron spin is therefore lifted via the hyperfine interaction with the nitrogen, allowing selective flip of the carbon nuclear spin $|\downarrow\rangle_C$ to polarize into $|\uparrow\rangle_C$ (green line in Fig. 2a). Initialization processes of the nitrogen and carbon nuclear spins are shown in Fig. 2b. The electron is again initialized into $|0\rangle_e$ with the red light resonant to the $|A_1\rangle$ state. The electron and carbon are then manipulated with a microwave optimized by GRAPE (GRadient Ascent Pulse Engineering)[30] and a radiowave to create entanglement between them into $|\Phi^+\rangle_{e,C} = \frac{1}{\sqrt{2}}(|+1, \uparrow\rangle_{e,C} + |-1, \downarrow\rangle_{e,C})$, which is one of four Bell states, along with the quantum circuit shown in Fig. 2c, where we define the SU(3) X gate that applies the X gate in the partial space spanned by $|a\rangle$ and $|b\rangle$ while retaining $|d\rangle$ as $X_{(\pi)}^{(|a\rangle, |b\rangle)} = |a\rangle\langle b| + |b\rangle\langle a| + |d\rangle\langle d|$. The Y gate applied to the spin-half carbon nuclear spin stands for Pauli operator σ_y.

Next, we allow the electron to absorb an incoming photon with arbitrary polarization $|\psi\rangle_p = \alpha|+1\rangle_p + \beta|-1\rangle_p$, which excites the electron into another spin-orbit correlated eigenstate $|A_1\rangle = \frac{1}{\sqrt{2}}(|+1, -1\rangle_{l,e} - |-1, +1\rangle_{l,e})^{23}$. The photon absorption projects the polarization state of the photon and the spin state of the electron into one of the Bell states as demonstrated in Kosaka et al.[23] Although the projection is probabilistic and allows only partial Bell state measurement, we repeat the transfer process until absorption into the $|A_1\rangle$ state stops after non-radiative relaxation into $|0\rangle_e$ of the orbital ground state. The projection of the prepared state composed of an arbitrary photon polarization $|\psi\rangle_p = \alpha|+1\rangle_p + \beta|-1\rangle_p$ and the electron-carbon entangled state $|\Phi^+\rangle_{e,C} = \frac{1}{\sqrt{2}}(|+1, \uparrow\rangle_{e,C} + |-1, \downarrow\rangle_{e,C})$ into the $|A_1\rangle$ state is described as

$$\langle A_1|\psi\rangle_l|\Phi^+\rangle_{e,C} = \frac{1}{2}\Big(\langle+1, -1|_{l,e} - \langle-1, +1|_{l,e}\Big)\big(\alpha|+1\rangle_l + \beta|-1\rangle_l\big)$$
$$\big(|+1, \uparrow\rangle_{e,C} + |-1, \downarrow\rangle_{e,C}\big)$$
$$= \frac{1}{2}\big(\beta|\uparrow\rangle_C - \alpha|\downarrow\rangle_C\big) = \frac{i}{2}\sigma_y|\psi\rangle_C,$$

(1)

where the photon polarization state $|\psi\rangle_p$ was substituted by the
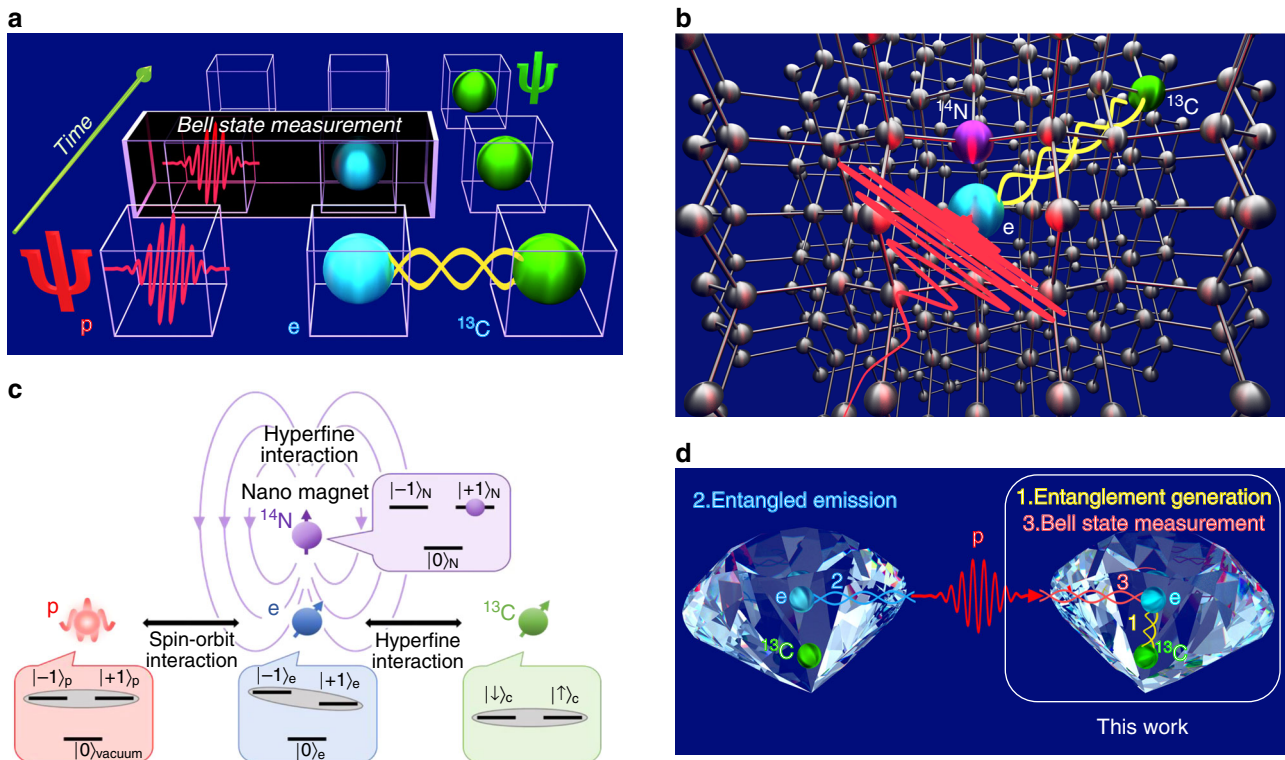
Fig. 1 Schematics of the quantum state transfer. **a** Protocol of the transfer scheme. We first prepare an entanglement between electron spin (e) and carbon nuclear spin (^{13}C) (bottom), and then measure photon polarization (p) and electron spin (e) in the Bell basis by photon absorption[23] (middle), which announces the success of the quantum state transfer from the photon into the carbon (top). **b** The lattice structure of diamond contains a nitrogen-vacancy (NV) center with surrounding carbon nuclear spins. An electron locates in the vacancy. **c** Energy level diagram of the photon based on the right/left ($|+1\rangle_p/|-1\rangle_p$) circular polarizations, the electron based on up/down ($|+1\rangle_e/|-1\rangle_e$) spin polarizations, and the carbon nuclear spin based on up/down ($|\uparrow\rangle_c/|\downarrow\rangle_c$) nuclear spin polarizations. The nitrogen impurity (^{14}N) polarized in $|+1\rangle_N$ nuclear spin polarization serves as a nanomagnet to apply a magnetic field only for the electron, allowing the preparation of entanglement between the hyperfine coupled electron and carbon spins under a zero magnetic field. The electron is then resonantly excited to a spin-orbit correlated eigenstate ($|A_1\rangle$) by photon absorption, allowing the measurement of the photon polarization and electron spin in the Bell basis to result in quantum state transfer from the photon into the carbon. **d** The supposed protocol of the one-way quantum repeater system with an NV center at each node. A photon is emitted from one node (left), leaving an electron entangled with the emitted photon. The success of the photon storage in the other node (right) establishes the entanglement between two adjacent nodes

electron orbital state $|\psi\rangle_l = \alpha|+1\rangle_l + \beta|-1\rangle_l$ since the photon polarization state p corresponds to the electron orbital state l via the angular momentum conservation or the polarization selection rule. The coefficient $\frac{i}{2}$ implies that success probability of the partial Bell state measurement is $|\frac{i}{2}|^2 = \frac{1}{4}$. However, the norm of the transferred nuclear spin becomes unity, which means that the nuclear spin state is in principle purified, after the post-selection of the electron spin state. The resulting nuclear spin state corresponds to the photon polarization state with the additional unitary operation σ_y.

Experiments. We first measure the phase correlation between the input photon and the transferred carbon to show that the transfer operation conserves the quantum coherence. In principle, the photon polarization state $|\psi\rangle_p = \frac{1}{\sqrt{2}}\left(|+1\rangle_p + e^{i\phi}|-1\rangle_p\right)$ should be transferred into the carbon nuclear spin polarization state $|\psi\rangle_C = \frac{1}{\sqrt{2}}\left(|\uparrow\rangle_C + e^{i(\pi-\phi)}|\downarrow\rangle_C\right)$ with the additional unitary transformation σ_y determined by Eq. (1). Figure 3a shows the photon polarization dependence of the carbon nuclear spin population measured in $|+\rangle_C - |-\rangle_C$ axis $\left(|\pm\rangle_C = \frac{1}{\sqrt{2}}\left(|\uparrow\rangle_C \pm |\downarrow\rangle_C\right)\right)$, which is obtained by measuring the photon count after the irradiation of a radiowave and a microwave followed by the red light resonant

to the $|E_x\rangle$ state (see Supplementary Fig. 5). Strong anti-phase correlation is observed as expected, indicating the quantum nature of the transfer.

To evaluate the fidelity of the quantum process during the state transfer, we prepare the six mutually-unbiased basis states of the photon polarization ($|+1\rangle_p, |-1\rangle_p, |+\rangle_p = \frac{1}{\sqrt{2}}(|+1\rangle_p + |-1\rangle_p), |-\rangle_p = \frac{1}{\sqrt{2}}(|+1\rangle_p - |-1\rangle_p), |+i\rangle_p = \frac{1}{\sqrt{2}}(|+1\rangle_p + i|-1\rangle_p), |-i\rangle_p = \frac{1}{\sqrt{2}}(|+1\rangle_p - i|-1\rangle_p)$) (Fig. 3b) and estimate the carbon nuclear spin state after the transfer based on the quantum state tomography. The Bloch vectors for the carbon nuclear spin states transferred from the six photon polarizations are reconstructed as shown in Fig. 3c. The fidelities projected into the ideal state reach 78 ± 2% on average, which well exceeds the classical limit of 67% (Fig. 3d). With the reconstructed Bloch vectors, we evaluated the quantum channel of the transfer based on the quantum process tomography as shown in Fig. 3e. The fidelity of the transfer process is estimated from the χ matrix defined as $\mathrm{Tr}[\chi^\dagger_{\mathrm{ideal}}\chi_{\mathrm{exp}}]$ to be 76%, indicating that the transfer channel maintains the quantum coherence.

The fidelity of the quantum state transfer degrades due to the imperfection of entanglement generation and Bell state measurement, which is caused by the incomplete initialization of spins (Fig. 3f), the mixing of orbital excited states due to the crystal strain (Fig. 3g), phase rotation during the Bell state
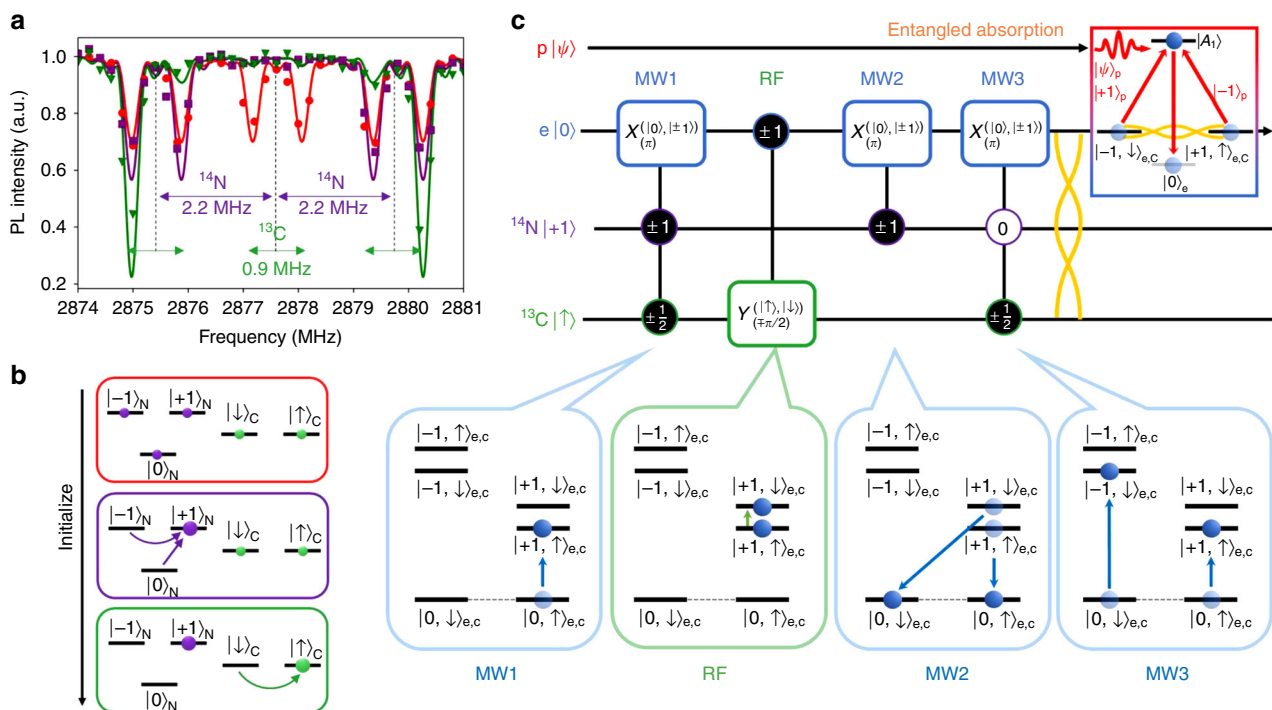
Fig. 2 Detailed scheme of the quantum state transfer. a Optically detected magnetic resonance (ODMR) spectra before and after the initialization process. The red, purple and green lines respectively show the spectrum before the initialization, after the initialization of only the nitrogen, and after initialization of both the nitrogen and carbon. The splittings of 2.2 MHz and 0.9 MHz are caused by the hyperfine interaction of the electron with the nitrogen and carbon, respectively. The achieved initialization fidelities are 94% for the nitrogen and 90% for the carbon. Error bars defined as the standard deviation of photon count are within point size. **b** Level diagrams showing populations for the nitrogen and the carbon nuclear spin corresponding to three steps in **a**. **c** Quantum circuit representing the transfer scheme. The controlled NOT(CNOT)-like symbols represent two or three qubit SU(3) gates, where the gates shown in the box are operated on the target qubit conditioned by the control qubit if the state is as given in the black circle or not as given in the white circle (double-sign corresponds). Below the circuit, energy level diagrams show the gate-induced transitions of the population in the ideally initialized case. Microwave (MW) 1 performs Toffoli-like π-gate to introduce the electron-carbon interaction, radio frequency (RF) performs controlled $\pi/2$ gate to generate a superposition of the carbon nuclear spin, MW2 performs controlled π-gate to eliminate the electron–carbon interaction, and MW3 again performs Toffoli-like π-gate to convert the superposition into an electron–carbon entanglement. Detection in the $|0\rangle_e$ state relaxed after resonant excitation into $|A_1\rangle$ post selects the photon polarization and electron spin states on a certain Bell state[23]

measurement (see Supplementary Note 2), and gate error. The initialization fidelity can be improved by repeating the initialization sequence. The effect of the crystal strain can be calibrated by identifying e_x and e_y, which are the x and y components of the crystal strain[23,26]. Phase rotation can be avoided by initializing the nitrogen nuclear spin into $|0\rangle_N$ before the transfer. Gate error can be improved by the development of a robust gate against inhomogenous broadening by the environmental nuclear spins.

Discussion
The hyperfine coupling of the nitrogen nuclear spin with the electron spin takes a constant value of around 2.2 MHz, while that of the carbon nuclear spin largely depends on its position, becoming smaller with increasing distance from the electron. By transferring the photon polarization state to the nuclear spin state of the carbon instead of the nitrogen, not only can the number of quantum memories which store the photon polarization state be increased but also the decoherence caused by the orbital excited state can be reduced by selecting a more distant carbon nuclear spin with smaller hyperfine coupling. Coupled carbon nuclear spins can also be used for a quantum memory that is robust against noise by utilizing a decoherence-protected subspace (DPS)[20].

The demonstration is independent of the photon number since we transferred the photon polarization state into the nuclear spin

polarization state of a single carbon. However, the single photon transfer[12] is important for the application of quantum key distribution with a single photon. Although around 10^4 photons are contained in a single pulse (200 nW, 20 ns), the probability of absorbing more than two photons is about 2.5% (see Supplementary Note 3).

Quantum efficiency of the state transfer is decomposed into the probability of photon absorption followed by relaxation into the $|0\rangle_e$ state and that of the $|0\rangle_e$ state detection. The overall efficiency demonstrated here is estimated to be 3×10^{-6} since the incoming light contains about 10^4 photons and the detected signal contains 3×10^{-2} photons in average (PL intensity: 500 counts per second; gate width: 60 μs). Both the absorption and emission probabilities can be increased at least seven times by implementing a solid immersion lens and much more by implementing an optical cavity. In principle, the absorption probability is limited to 25% by the partial Bell state measurement in addition to 40% by the relaxation into the $|0\rangle_e$ state, but the detection probability can be 100% with the single-shot projective measurement. Even though the efficiency is not perfect, the state transfer scheme allows post-selection of the succeeded transfer, leading to high fidelity transfer independent of the absorption efficiency. The transfer rate can be drastically increased by introducing NV integrated memories controlled with optical holonomic quantum gates[26–29]. The transfer can be also deterministic in principle by introducing a feedback loop with a tunable waveplate[31].
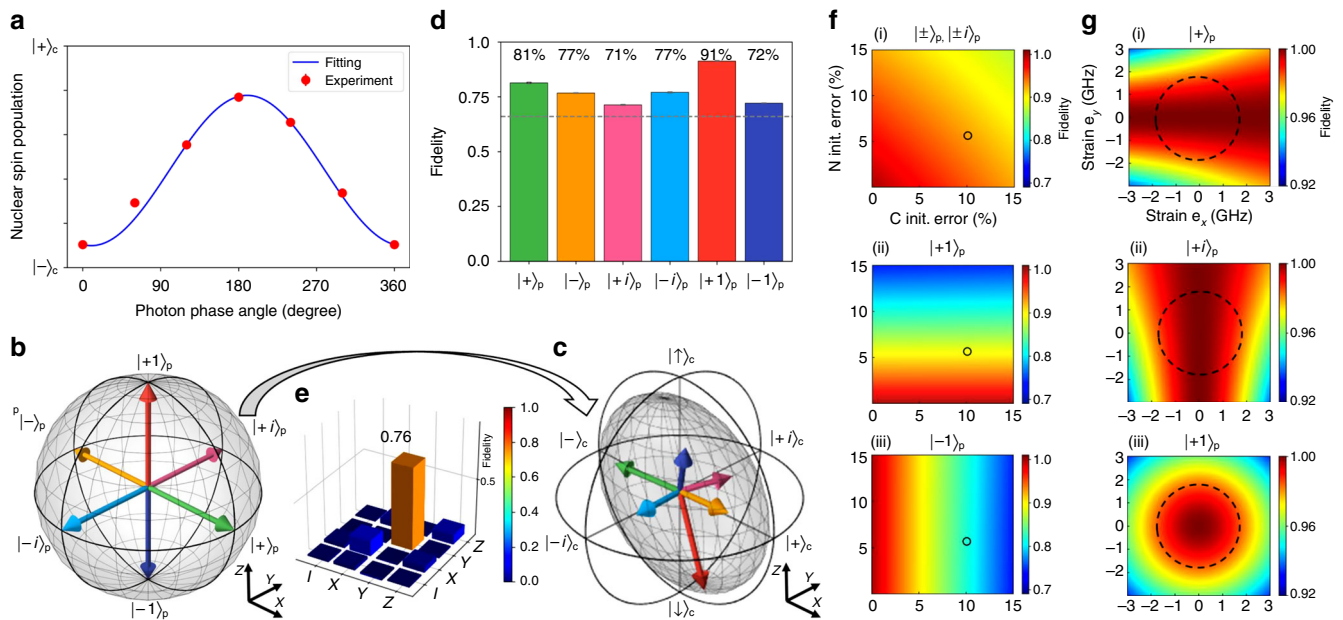
Fig. 3 Experimental demonstration of the quantum state transfer. **a** Correlation between the photon phase angle (twice the polarization angle) and the carbon nuclear spin population measured in $|+\rangle_C - |-\rangle_C$ axis, which is converted into the population of the electron spin ancilla state. **b** The Poincare sphere representation of the polarization state of the input light. **c** The Bloch sphere representation of the quantum state stored in the carbon nuclear spin reconstructed by the quantum state tomography. Six basis polarization states of the incoming photon are transferred into the memory carbon. The meshed frame shows the distorted Bloch sphere estimated by the process tomography measurements shown in **e**. **d** The state fidelities of the carbon for the six basis polarization states defined by $\text{Tr}[\rho^\dagger_{\text{ideal}}\rho_{\text{exp}}]$. The averaged state fidelity is 78%, which well exceeds the classical limit of 67%. **e** Matrix representation of the quantum process tomography for the state transfer. The matrix elements χ_{exp} are calculated based on the transferred states shown in **c**. The transfer process fidelity defined by $\text{Tr}[\chi^\dagger_{\text{ideal}}\chi_{\text{exp}}]$ is 76%. Error bars defined as the standard deviation of photon count in **a**, **c**–**e** are within point size (<2%). **f** Simulated dependence of the transfer fidelity on the initialization fidelities for the carbon and nitrogen nuclear spins for the photon polarizations **(i)**, $|+\rangle_p, |-\rangle_p, |+i\rangle_p, |-i\rangle_p$, **(ii)**, $|+1\rangle_p$, and **(iii)**, $|-1\rangle_p$. Solid circles represent the ranges of the initialization errors for the demonstration. **g** Simulated dependence of the transfer fidelity on the two vector components of the crystal strain for the photon polarizations **(i)**, $|+\rangle_p$, **(ii)**, $|+i\rangle_p$, and **(iii)**, $|+1\rangle_p$. Dashed circles represent the ranges of the crystal strain for the demonstration

We demonstrated reliable quantum state transfer of photon polarization into a carbon nuclear spin coupled to an NV center in diamond based on photon-electron Bell state measurement by photon absorption[23]. Detection of the electron relaxed in the spin ground state post-selected the transfer of the photonic quantum state in the long-lived carbon memory without revealing or destroying the stored quantum information. This demonstration shows that the state transfer scheme can be applied not only for a spin 1 system but also for a spin half system. The scheme allows integrated quantum memories to be individually addressed in order to realize scalable quantum repeaters for long-haul quantum communications and distributed quantum computers.

Methods

Sample and experimental conditions. We used a negatively charged NV center in a type-II a bulk diamond made by Element Six. The sample has a <001> crystal orientation. We adjusted the position of a permanent magnet in the direction along the geomagnetism to achieve a zero magnetic field by reducing the Zeeman splitting in the ODMR spectrum within 0.1 MHz. The NV center was located about 30 μm below the surface and has a crystal strain of about 1.8 GHz, which was estimated by the splitting between the $|E_x\rangle$ and $|E_y\rangle$ transitions in the photo-luminescence spectrum. The polarization of the photon was calibrated for the NV center to be properly applied by considering the Hamiltonian including the off-alignment between the optical axis and the crystal orientation[26].

Microwave setup. A 25 μm copper wire mechanically attached to the surface of the diamond was used to apply a microwave and a radiowave. A shaped microwave around 2877 MHz optimized by GRAPE[30] for manipulating the electron spin was generated by up-converting a local oscillator (2776 MHz) with a radiowave around 100 MHz generated by an arbitrary wave generator (Keysight 33622A). A radio-wave around 0.9–7 MHz for manipulating the nuclear spin was directly generated by an arbitrary wave generator (Keysight 33522A).

Laser setup. A green laser (wavelength: 532 nm; power: 150 μW) was pulsed by an AOM (acousto-optic modulator) with an extinction ratio of about 10^3. A red tunable laser, whose wavelength (~637.2 nm) was set to be resonant to $|A_1\rangle$ was branched into three beams. Two of them were pulsed by both an AOM and EOM (electro-optic modulator) with an extinction ratio of about 10^9 and were used for initialization of the electron into $|0\rangle_e$ (power: ~30 nW) and for the transfer of photon polarization into carbon nuclear spin (power: ~200 nW), respectively. The other beam was pulsed only by an AOM with an extinction ratio of about 10^4 together with an EOM as a phase modulator to set its frequency to resonant to $|E_x\rangle$ and used for the readout of $|0\rangle_e$ (power: ~5 nW). Another red tunable laser (wavelength: ~637.2 nm; power: ~500 nW) was pulsed by both an AOM and EOM with an extinction ratio of about 10^9 and a frequency set to be resonant to $|A_2\rangle$, and was used for the CPT of the electron into $|+1\rangle_e$. Arbitrary polarization was set using a pair of variable wave plates placed at the end of each beam line.

Data availability

The data that support the findings of this study are available from the corresponding author upon request.

References

1. Bennett, C. H. et al. Teleporting an unknown quantum state via dual classical and einstein-podolsky-rosen channels. *Phys. Rev. Lett.* **70**, 1895–1899 (1993).
2. Bouwmeester, D. et al. Experimental quantum teleportation. *Nature* **390**, 575–579 (1997).
3. Duan, L. M., Lukin, M. D., Cirac, J. I. & Zoller, P. Long-distance quantum communication with atomic ensembles and linear optics. *Nature* **414**, 413–418 (2001).

4. Gisin, N., Ribordy, G., Tittel, W. & Zbinden, H. Quantum cryptography. *Rev. Mod. Phys.* **74**, 145–195 (2002).
5. Kimble, H. J. The quantum internet. *Nature* **453**, 1023–1030 (2008).
6. Ladd, T. D. et al. Quantum computers. *Nature* **464**, 45–53 (2010).
7. Briegel, H. J., Dür, W., Cirac, J. I. & Zoller, P. Quantum repeaters: the role of imperfect local operations in quantum communication. *Phys. Rev. Lett.* **81**, 5932–5935 (1998).
8. Childress, L., Taylor, J. M., Sorensen, A. S. & Lukin, M. D. Fault-tolerant quantum communication based on solid-state photon emitters. *Phys. Rev. Lett.* **96**, 070504 (2006).
9. Jiang, L. et al. Quantum repeater with encoding. *Phys. Rev. A* **79**, 032325 (2009).
10. Pfaff, W. et al. Unconditional quantum teleportation between distant solid-state quantum bits. *Science* **345**, 532–535 (2014).
11. Yang, S. et al. High fidelity transfer and storage of photon states in a single nuclear spin. *Nat. Photon.* **10**, 507–511 (2016).
12. Delteil, A., Sun, Z., Fält, S. & Imamoğlu, A. Realization of a cascaded quantum system: Heralded absorption of a single photon qubit by a single-electron charged quantum dot. *Phys. Rev. Lett.* **118**, 177401 (2017).
13. Humphreys, P. C. et al. Deterministic delivery of remote entanglement on a quantum network. *Nature* **558**, 268–273 (2018).
14. Broadbent, A., Fitzsimons, J. & Kashefi, E. Universal blind quantum computation. In Proceedings of the 50th Annual IEEE Symposium on Foundations of Computer Science (FOCS '09) 517–526 (IEEE Computer Society, Los Alamitos, USA, 2009).
15. Teraji, T., Taniguchi, T., Koizumi, S., Koide, Y. & Isoya, J. Effective use of source gas for diamond growth with isotopic enrichment. *Appl. Phys. Express* **6**, 055601 (2013).
16. Dutt, M. V. G. et al. Quantum register based on individual electronic and nuclear spin qubits in diamond. *Science* **316**, 1312–1316 (2007).
17. Neumann, P. et al. Multipartite entanglement among single spins in diamond. *Science* **320**, 1326–1329 (2008).
18. Waldherr, G. et al. Quantum error correction in a solid-state hybrid spin register. *Nature* **506**, 204–207 (2014).
19. Cramer, J. et al. Repeated quantum error correction on a continuously encoded qubit by real-time feedback. *Nat. Commun.* **7**, 11526 (2016).
20. Reiserer, A. et al. Robust quantum-network memory using decoherence-protected subspaces of nuclear spins. *Phys. Rev. X* **6**, 021040 (2016).
21. Abobeih, M. H. et al. One-second coherence for a single electron spin coupled to a multi-qubit nuclear-spin environment. *Nat. Commun.* **9**, 2552 (2018).
22. Sekiguchi, Y. et al. Geometric spin echo under zero field. *Nat. Commun.* **7**, 11668 (2016).
23. Kosaka, H. & Niikura, N. Entangled absorption of a single photon with a single spin in diamond. *Phys. Rev. Lett.* **114**, 053603 (2015).
24. Togan, E. et al. Quantum entanglement between an optical photon and a solid-state spin qubit. *Nature* **466**, 730–734 (2010).
25. Kosaka, H. et al. Coherent transfer of light polarization to electron spins in a semiconductor toward quantum media conversion. *Phys. Rev. Lett.* **100**, 096602 (2008).
26. Sekiguchi, Y., Niikura, N., Kuroiwa, R., Kano, H. & Kosaka, H. Optical holonomic single quantum gates with a geometric spin under a zero field. *Nat. Photon.* **11**, 309–314 (2017).
27. Zhou, B. B. et al. Holonomic quantum control by coherent optical excitation in diamond. *Phys. Rev. Lett.* **119**, 140503 (2017).
28. Ishida, N. et al. Universal holonomic single quantum gates over a geometric spin with phase-modulated polarized light. *Opt. Lett.* **43**, 2380–2383 (2018).
29. Nagata, K., Kuramitani, K., Sekiguchi, Y. & Kosaka, H. Universal holonomic quantum gates over geometric spin qubits with polarised microwaves. *Nat. Commun.* **9**, 3227 (2018).
30. Khaneja, N., Reiss, T., Kehlet, C., Schulte-Herbrüggen, T. & Glaser, S. J. Optimal control of coupled spin dynamics: design of NMR pulse sequences by gradient ascent algorithms. *J. Magn. Reson.* **172**, 296–305 (2005).
31. Scharfenberger, B., Kosaka, H., Munro, W. J. & Nemoto, K. Absorption-based quantum communication with NV centres. *New J. Phys.* **17**, 103012 (2015).

Acknowledgements

Author contributions

The experiment was designed and analysed by K.T., R.K., H. Kano and H. Kosaka. Measurements were made by K.T., R.K. and H. Kano. Y. S. supported experiments in technical matters. H. Kosaka supervised experiments. K. T. and H. Kosaka wrote the paper.

Additional information

Supplementary information accompanies this paper at https://doi.org/10.1038/s42005-019-0158-0.

Competing interests: The authors declare no competing interests.

Reprints and permission information is available online at http://npg.nature.com/reprintsandpermissions/

Publisher's note: Springer Nature remains neutral with regard to jurisdictional claims in published maps and institutional affiliations.